

AFTER RUNAWAY: THE TRANS-HILL STAGE OF PLANETESIMAL GROWTH

YORAM LITHWICK¹

Draft version March 19, 2013

ABSTRACT

When planetesimals begin to grow by coagulation, they enter an epoch of runaway, during which the biggest bodies grow faster than all the others. The questions of how runaway ends and what comes next have not been answered satisfactorily. Here we show that runaway is followed by a ‘trans-hill stage’ that commences once the bodies become trans-hill, i.e. once the Hill velocity of the bodies that dominate viscous stirring matches the random speed of the small bodies they accrete. Subsequently, the small bodies’ speed grows in lockstep with the big bodies’ sizes, such that the bodies remain in the trans-hill state. Trans-hill growth is crucial for determining the efficiency of growing big bodies, as well as their growth timescale and size spectrum.

We work out the properties of trans-hill growth analytically and confirm these numerically. Trans-hill growth has two sub-stages. In the earlier one, collisional cooling is irrelevant, in which case the efficiency of forming big bodies remains very low (0.1% in the Kuiper belt) and their mass spectrum is flat. This explains results from previous coagulation simulations for both the Kuiper belt and the asteroid belt. The second sub-stage commences when small bodies begin to collide with one another. Collisional cooling then controls the evolution, in which case the efficiency of forming big bodies rises, and their size spectrum becomes more top-heavy.

Trans-hill growth terminates in one of two ways, depending on parameters. First, mutual accretion of big bodies can become significant and conglomeration proceeds until half the total mass is converted into big bodies. This mode of growth may explain the size distributions of minor bodies in the Solar System, and is explored in forthcoming work. Second, if big bodies become separated by their Hill radius, oligarchy commences. This mode likely precedes the formation of fully-fledged planets.

1. INTRODUCTION

Our understanding of how planets form remains inadequate. This hinders attempts to explain the many recent discoveries of extra-solar planets, proto-planetary disks and debris disks. Planet formation is often decomposed into a number of stages. In the first stage, “planetesimals” form out of dust embedded in protoplanetary disks. How that happens is highly uncertain because it depends on complicated physics such as how particles stick and how they interact with a turbulent gas disk (see Chiang & Youdin 2010, for a review). The initial planetesimals are often assumed to be kilometer-sized, but they could be much smaller or larger than that (e.g., Johansen et al. 2007). In the second stage, sometimes called coagulation, the planetesimals attract one another gravitationally, merge and grow. This stage is more easily understood than the first, because the dominant physical process is simply gravity (see Goldreich et al. 2004b, hereafter GLS, for a review). Nonetheless, past studies have given different, sometimes even conflicting, views on this process. What happens after coagulation depends on local conditions. Just beyond the snow-line, coagulation is thought to produce cores that then accrete massive gaseous atmospheres to form gas giants (Pollack et al. 1996). In the terrestrial zone, coagulation produces dozens of sub-earth-sized bodies that then undergo a velocity instability once they have accreted half the planetesimals, leading to an epoch of large-scale chaos and giant impacts (Chambers & Wetherill 1998;

Goldreich et al. 2004a). And in the asteroid belt, Kuiper belt, and extra-solar debris disks, coagulation is thought to have been incomplete, perhaps because the coagulating planetesimals were excited by exterior planets before forming planets themselves, or because the initial surface density was very low.

It is the second stage, coagulation, that is the topic of this paper. Our goal is to build a theory that explains the properties of bodies that ultimately form, such as their number, size distribution, formation timescale, and *efficiency*, where the efficiency is the fraction of mass in the original planetesimals that ends up in big bodies. This theory can then be compared against observations, especially of the asteroid and Kuiper belts, whose large bodies are thought to be frozen remnants of the coagulation process.

Coagulation is usually studied with numerical simulations. Starting from an assumed initial state, the planetesimals begin to merge. The merging rate depends on gravitational focusing factors, which are functions of the relative speeds. The relative speeds are in turn affected by a variety of two-body processes such as viscous stirring, dynamical friction, and inelastic collisions. While there have been many such simulations, using a variety of techniques (e.g., Greenberg et al. 1978; Wetherill & Stewart 1989; Kokubo & Ida 1998; Weidenschilling et al. 1997; Kenyon & Luu 1999; Inaba et al. 2001; Morbidelli et al. 2009; Ormel et al. 2010b; Weidenschilling 2011; Schlichting & Sari 2011), the simulations are complicated, and hence it is often difficult to disentangle the various effects in order to understand the results and be confident that they are correct. Moreover, the results from different

¹ Department of Physics and Astronomy, Northwestern University, Evanston, IL 60208 and Center for Interdisciplinary Exploration and Research in Astrophysics (CIERA)

groups do not always agree (e.g. Morbidelli et al. 2009; Weidenschilling 2011). Compounding the difficulty are a number of fundamental uncertainties—such as the unknown initial size and velocity distributions, how collisional fragmentation occurs, and when are gaps opened in the circumstellar disk. A theory for coagulation would be desirable to guide and interpret simulations, and to determine how sensitive the results are to assumptions.

Early coagulation simulations led to the discovery of runaway growth, in which the size distribution quickly develops a tail extending to extremely large sizes (Safronov 1972; Greenberg et al. 1978; Wetherill & Stewart 1989). Runaway occurs because, with gravitational focusing included, the growth rate of bodies ($d \ln R/dt$) can be an increasing function of their radius R (see also Section 3.1, below). This implies that the largest bodies continue to double to infinite size before smaller ones double a single time. The properties of runaway growth have been studied analytically (e.g., Lee 2000; Malyskin & Goodman 2001). A variety of theories have been proposed to explain how runaway growth ends, and what comes next (e.g., Ida & Makino 1993; Kokubo & Ida 1998; Ormel et al. 2010b; Schlichting & Sari 2011). It is often thought that runaway accretion is followed by self-regulated oligarchic growth, during which each big body heats its own food. We show here, however, that there is a critical intervening stage of growth, which we call the trans-hill stage.

In the absence of an understanding of the trans-hill stage, previous studies (e.g., GLS) could not explain two key results of conglomeration simulations: the size spectrum and the formation efficiency of large bodies. Here we show that trans-hill growth is a critical stage for determining these, and based on our analytical understanding we provide simple scalings to explain results of previous numerical simulations.

During trans-hill growth, conglomeration can be categorized as collisionless or collisional, with very different outcomes for formation efficiency and size spectrum. In the collisionless case small bodies rarely collide, while in the collisional one the small bodies' dispersion is reduced by frequent inelastic collisions. Collisionless growth has been often simulated before, but without clear interpretation. Collisional growth, on the other hand, is just starting to be explored (Weidenschilling 2011; Shannon et al. 2013b). Our study here provides a unified framework for both regimes.

The structure of this paper is as follows. In Section 2 we present the equations of motion. We re-write these in Appendix A in a form suitable for numerical integration or analytic solution. In Section 3 we review runaway growth, and show that it inexorably transitions into trans-hill growth. We then derive qualitatively the properties of trans-hill growth. In Section 4 we present exact solutions of trans-hill growth, using numerical integrations as well as analytical self-similar solutions (derived in Appendix B). Section 5 describes what comes after trans-hill growth. Section 6 examines our assumptions and delineates their range of validity. Section 7 discusses applications of our theory to the asteroid and Kuiper belts, and compares with a number of earlier papers. Section 8 summarizes.

Shannon et al. (2013a,b) present particle-in-box simu-

lations in both the collisionless and collisional regimes, without the restrictive assumptions made in the present paper. The results there confirm and refine those of this study. The collisional paper in particular focuses on the formation of the Cold Classical Kuiper belt. It presents a new picture where KBOs form out of a very low mass planetesimal disk (the “minimum mass Kuiper belt”), 100 times less massive than the minimum mass solar nebula.

2. ASSUMPTIONS AND EQUATIONS OF MOTION

We examine first the interactions between two groups of bodies, big ones and small ones, before proceeding to consider a distribution of bodies. This ‘two-groups’ approximation has been described by GLS and we follow their notation. Big bodies have radius R and surface density Σ ; small bodies have radius s , surface density σ , and velocity dispersion u . All bodies have the same bulk density, with $\rho \sim 1 \text{ g cm}^{-3}$. We make the following assumptions, and then check for self-consistency in Section 6:

1. The small bodies' random speed u satisfies

$$\alpha^{1/2} < u/v_H < \alpha^{-1/2}, \quad (1)$$

where α is the ratio of all bodies' physical radius to their Hill radius (R/R_H) and v_H is the big bodies' Hill velocity. Explicitly,

$$\alpha \equiv \frac{R}{R_H} \sim \frac{R_\odot}{a} \ll 1, \quad (2)$$

where the expression R_\odot/a (the ratio of the Sun's radius to the semimajor axis) follows from the fact that the Sun's density is comparable to that of solid bodies. In the asteroid belt $\alpha \sim 2 \times 10^{-3}$, while in the Kuiper belt $\alpha \sim 10^{-4}$. In addition,

$$v_H \sim R\sqrt{G\rho\alpha}, \quad (3)$$

The small bodies' speed can be sub- or super-hill with respect to the big bodies ($u < v_H$ or $u > v_H$), subject to the constraints that u is less than the surface escape speed from the big bodies ($u < \alpha^{-1/2}v_H$) and that small bodies are not accreted in the “very thin disk” accretion regime ($u > \alpha^{1/2}v_H$).

2. The big bodies' random speed v is sub-hill ($v < v_H$).
3. $\Sigma \ll \sigma$, and so σ is essentially the total surface density, and is treated as a constant during the growth. More stringently, we assume that big bodies grow only by accreting small ones. This is certainly true at early times, when there are only a few big bodies.
4. The small bodies' size s is a constant parameter. Small bodies do not grow, and they also do not fragment in collisions.
5. More than a single big body dominates viscous stirring at a given distance from the star, and hence the big body number distribution can be treated as a continuous function. This assumption is violated when oligarchy commences.

With the above assumptions, big bodies grow by accreting small ones at the rate (GLS),

$$\frac{1}{R} \frac{dR}{dt} = \frac{\sigma\Omega}{\rho R} \alpha^{-1} \begin{cases} (v_H/u)^2, & \text{if } u > v_H \\ v_H/u, & \text{if } u < v_H \end{cases} \quad (4)$$

where Ω is the orbital angular speed around the Sun.

For the evolution of u , small bodies are damped by inelastic collisions amongst themselves, and are viscously stirred by the big bodies. The net rate is (GLS).

$$\frac{1}{u} \frac{du}{dt} = -\frac{\sigma\Omega}{\rho s} + \frac{\Sigma\Omega}{\rho R} \alpha^{-2} \begin{cases} (v_H/u)^4, & \text{if } u > v_H \\ v_H/u, & \text{if } u < v_H \end{cases} \quad (5)$$

If the first term on the right hand side is important the system is collisional, otherwise it is collisionless.

The above equations for two groups of bodies are easily extended to a continuous distribution of big bodies. We denote the cumulative number distribution of big bodies as $N(> R)$. Because we neglect accretion of big bodies, the number of big bodies remains constant as they grow. In other words, N satisfies the continuity equation

$$\frac{\partial N}{\partial t} + V \frac{\partial N}{\partial R} = 0, \quad (6)$$

where $V \equiv dR/dt$ is given in Equation (4). In place of Equation (5), we replace $\Sigma \rightarrow d\Sigma$, then set

$$\frac{d(\Sigma/\sigma)}{d \ln R} = R^3 \frac{d(N/\eta)}{d \ln R} \quad (7)$$

and integrate over dR . Here η is a constant; we shall not need its value because it is only the ratio N/η that is dynamically significant.

Equations (4)–(7) are the equations of motion. We solve them both analytically (Appendix B) and numerically (see method in Appendix A). But before presenting the exact solutions, we first use simple analytical arguments to show that runaway growth inexorably converges towards ‘trans-hill growth’. This realization gives rise to a number of our main results on the mass spectrum and formation efficiency (Section 3), as verified by our exact solutions (Section 4).

3. FROM RUNAWAY TO TRANS-HILL GROWTH

3.1. Runaway

We summarize the traditional picture of how runaway growth proceeds (e.g., Ida & Makino 1993). It is typically assumed that bodies of some characteristic size (here, s) emerge from a dissipating protoplanetary gas disk. The value of s is highly uncertain, since it is not even understood how the bodies formed.

On the timescale that bodies of size s collide, $\rho s/(\sigma\Omega)$, they stir each other up to their surface escape speed, $u \sim s\sqrt{G\rho} \sim \alpha^{-1/2}v_H|_s$ (Equation (5)), where $v_H|_s$ is the Hill velocity for bodies of size s . On the same timescale, they grow in mass by accreting each other.² The evolution of those bigger bodies (radius labelled by R) proceeds in the runaway regime. This is because the growth rate when $u > v_H$ is an increasing function of

² It is possible that some bodies grow to very large sizes before u is stirred up to the small bodies’ escape speed, depending on the details of how the small bodies formed. We discuss the effect of this on trans-hill growth below.

R , i.e. $d \ln R/dt \propto R$ (Equations (3) and (4)). Thus, comparing two big bodies with different values of R , the bigger one will double in size faster than the smaller one, and then will double again even faster. It will ultimately reach infinite size—or violate one of the assumptions made—before the smaller one has doubled a single time.

3.2. From Runaway to Trans-hill Growth

Runaway growth requires $u > v_H$. Since v_H increases linearly with R , when runaway bodies get big enough their Hill velocity can be sufficiently large that $u < v_H$. In that sub-hill case, big bodies grow in the ‘neutral’ regime (GLS), i.e., since the growth rate is independent of R (Equation (4)), the distribution function of big bodies $N(> R)$ maintains its shape while moving to larger R .

In general, some big bodies grow in the runaway regime, and others in the neutral regime, depending on their radius:

$$\text{runaway growth, if } R < R_{\text{tran}} \quad (8)$$

$$\text{neutral growth, if } R > R_{\text{tran}}, \quad (9)$$

where the trans-hill radius is

$$R_{\text{tran}} \equiv \frac{u}{\sqrt{G\rho\alpha}}, \quad (10)$$

which is the radius of the big bodies that have Hill velocity equal to the small bodies’ speed ($v_H|_{R_{\text{tran}}} = u$).

As we now show, the big bodies’ distribution function is always driven to the trans-hill state, defined as $R_{\text{stir}} \sim R_{\text{tran}}$, where R_{stir} is the radius of the big bodies that dominate viscous stirring. Subsequently, the small body velocity dispersion and the size of the bodies that dominate stirring grow in lockstep, maintaining $R_{\text{stir}} \sim R_{\text{tran}}$. Our argument proceeds by considering the two initial situations, $R_{\text{stir}} \ll R_{\text{tran}}$ or $R_{\text{stir}} \gg R_{\text{tran}}$, in turn.

- If initially $R_{\text{stir}} \ll R_{\text{tran}}$ (Fig. 1), as is relevant for the early phases of planetesimal growth, the small bodies are super-hill with respect to the stirrers. All big bodies with $R > R_{\text{stir}}$ repeatedly double in size before the stirring bodies (R_{stir}) have doubled once.³ This runaway produces new bodies that contribute more to stirring ($\propto \Sigma R^3$, Equation (5)) than the original stirrers and these new bodies come to dominate the stirring. Although R_{tran} also grows due to viscous stirring, R_{stir} grows faster, as we presently show. The growth of R_{stir} is at least as fast as the size doubling rate at R_{stir} , $d \ln R_{\text{stir}}/dt \geq d \ln R/dt|_{R=R_{\text{stir}}}$. Meanwhile, the heating of small bodies increases R_{tran} as $d \ln R_{\text{tran}}/dt \sim d \ln u/dt$ (Equation (5)). We first focus on the collisionless case, inserting $s = \infty$ into Equation (5) to get

$$\frac{d \ln R_{\text{stir}}/dt}{d \ln R_{\text{tran}}/dt} \geq \left(\frac{\alpha\sigma}{\Sigma_{\text{stir}}} \right) \left(\frac{R_{\text{tran}}}{R_{\text{stir}}} \right)^2,$$

where Σ_{stir} is the mass density at R_{stir} . If the efficiency of formation is limited by $\Sigma_{\text{stir}}/\sigma \sim \alpha$, as

³ Even though very large bodies, with radius above R_{tran} , grow in the neutral regime, their doubling rate also exceeds that of the stirring bodies.

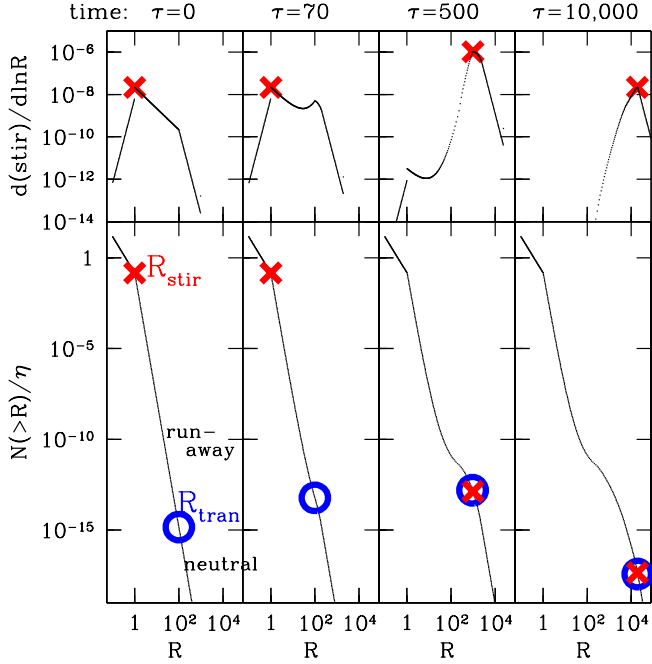


Figure 1. From Runaway to Trans-hill Growth. Result of a numerical integration of the collisionless equations of motion (Equations (4)–(7) with $s = \infty$ and $\alpha = 10^{-4}$). The leftmost panels (top and bottom) show the initial conditions, where the bottom panel is the big body distribution function, and the top panel is the stirring rate per $\ln R$ (the right-hand side of Equation (5) with $\Sigma \rightarrow |d\Sigma/d\ln R|$). The red cross marks R_{stir} , defined to be the maximum of the curve in the top panel. The blue circle marks $R_{\text{tran}} \equiv u/\sqrt{G\rho\alpha}$. Initially u is the escape speed from bodies with $R = 1$ (i.e. $R_{\text{tran}} = \alpha^{-1/2} = 100$). The panels at subsequent times ($\tau = 70, 500, 10^4$, with τ the scaled time, $\tau \equiv t\sigma\Omega/(\rho\alpha)$; see Equation (A1)) show that the system evolves from $R_{\text{stir}} \ll R_{\text{tran}}$ to the trans-hill state $R_{\text{stir}} \sim R_{\text{tran}}$, and thereafter remains trans-hill.

we show below to be true for the collisionless case, with time R_{stir} catches up to R_{tran} . An alternative argument showing that R_{stir} grows faster is that if there were no bodies bigger than the original stirring bodies, then, as long as the small bodies are collisionless, the stirring bodies grow at the same rate as u , i.e. $d\ln R_{\text{stir}}/dt \sim d\ln R_{\text{tran}}/dt$. But by the nature of runaway growth, the bodies bigger than the original R_{stir} must grow faster than that. We conclude that, in the collisionless regime, the ratio $R_{\text{stir}}/R_{\text{tran}}$ approaches unity. The simulation in Figure 1 confirms this.

The same conclusion applies to the collisional case as well, because collisional damping forces u (and hence R_{tran}) to grow even more slowly than in the collisionless case. Hence R_{stir} catches up with R_{tran} even more quickly.

- If initially $R_{\text{tran}} \ll R_{\text{stir}}$, the stirring bodies grow in the neutral regime. Focusing first on the collisional case, Equation (5) with $u \leq v_H$ implies that $\Sigma_{\text{stir}} \propto u \propto R_{\text{tran}}$. Because the stirring bodies grow neutrally, the shape of the distribution function near R_{stir} does not change as R_{stir} grows, and hence the number of stirring bodies does not change, i.e., $\Sigma_{\text{stir}} \propto R_{\text{stir}}^3$. As a result, $R_{\text{stir}}/R_{\text{tran}} \propto 1/R_{\text{stir}}^2$, which decreases with time towards unity. The same

conclusion applies to the collisionless regime, because in that case u , and hence R_{tran} , will increase even faster.

3.3. How Trans-hill Growth Proceeds

We have shown that during runaway the big bodies' distribution is driven towards the trans-hill state

$$R_{\text{stir}} \sim R_{\text{tran}}, \quad (11)$$

or equivalently

$$u \sim v_H|_{R_{\text{stir}}}, \quad (12)$$

and that after that the big bodies continue to grow in this state. We call this new stage of growth *trans-hill growth*.

During trans-hill growth, all bodies with $R < R_{\text{stir}}$ do not grow significantly because those with $R > R_{\text{stir}}$ double faster than they do, i.e. the distribution becomes frozen in time at small R . Furthermore, bodies with $R > R_{\text{stir}}$ follow neutral growth, and their distribution maintains its shape. Throughout, $R_{\text{tran}} \sim R_{\text{stir}}$, and both increase with time, following (Equation 4)

$$R_{\text{stir}} \sim \frac{\sigma\Omega}{\rho\alpha}t. \quad (13)$$

We may also evaluate the mass fraction in bodies that dominate stirring, $\Sigma_{\text{stir}}/\sigma$, as a function of R_{stir} . We find, dropping the “stir” subscripts,

$$\frac{\Sigma}{\sigma} \sim \begin{cases} \alpha, & \text{collisionless } (R < s/\alpha) \\ \alpha^2 R/s, & \text{collisional } (R > s/\alpha) \end{cases}, \quad (14)$$

where the collisionless expression above follows from setting $d\ln u/dt \sim d\ln R_{\text{stir}}/dt$ and dropping the collisional term in Equation (5); and the collisional expression follows from dropping the left-hand side of Equation (5).⁴ The transition from collisionless to collisional trans-hill evolution occurs once R_{stir} exceeds a critical size

$$R_{\text{stir}} \gtrsim R_{\text{stir}}^{(\text{col})} = s/\alpha, \quad (15)$$

because beyond this size, small bodies collisionally cool faster than the growth of trans-hill bodies. This transition occurs at $t \sim \rho s/(\sigma\Omega)$, i.e., the small bodies' collision time.

Following conventional practice, we define the power-law index q of the differential number distribution

$$\frac{dN}{dR} \propto R^{-q} \propto \Sigma(>R)R^{-4}, \quad (16)$$

in which case we have

$$q = \begin{cases} 4, & \text{collisionless } (R < s/\alpha) \\ 3, & \text{collisional } (R > s/\alpha) \end{cases} \quad (17)$$

4. EXACT SOLUTIONS

We present exact solutions of the equations of motion. We first summarize the analytical self-similar solutions to

⁴ Because the spectrum is frozen at small R , Equation (14) gives not only the temporal evolution of Σ_{stir} , but also the frozen spectrum at $R < R_{\text{stir}}$ —that is why we drop the “stir” subscript.

these equations (derived in Appendix B), and then integrate the equations numerically for a number of cases—both when the initial conditions are as given by the self-similar solution, and for more realistic initial conditions.

4.1. Analytical self-similar solutions

It is shown in the appendices that the equations of motion (Equations (4)–(7), or equivalently Equations (A1)–(A4)) admit self-similar solutions when the radii R are scaled relative to R_{tran} , and when the stirring is either in the collisionless or collisional regime. In either case, there is a single free parameter, the power-law exponent for bodies that grow neutrally, i.e., the value of γ such that $N \propto R^{-\gamma}$ at $R > R_{\text{tran}}$. The value of γ remains frozen in time by the nature of neutral growth, as long as the assumptions of Section 2 remain valid. However, the value of γ in real disks is difficult to ascertain from first principles, and likely depends both on how the bodies form and on the early stages of coagulation. Fortunately, the solutions are quite insensitive to γ as long as $\gamma \gg 3$, or equivalently as long as stirring is dominated by bodies at finite sizes, not by those with $R = \infty$.

The exact self-similar solutions (displayed in Equations (B8) and (B12) and graphed in Figures 2 and 3) confirm what was derived qualitatively in Section 3. In particular, from the functional dependence of N on R , one sees that stirring is maximized near $R \sim R_{\text{tran}}$, and hence $R_{\text{stir}} \sim R_{\text{tran}}$. In addition, the differential mass fraction at $R \ll R_{\text{tran}}$ is consistent with Equation (14):

$$\frac{d}{d \ln R} \frac{\Sigma}{\sigma} = -3g_{\text{nocol}}(\gamma)\alpha, \text{ collisionless} \quad (18)$$

$$\frac{d}{d \ln R} \frac{\Sigma}{\sigma} = -2g_{\text{col}}(\gamma)\alpha^2 \frac{R}{s}, \text{ collisional}. \quad (19)$$

The order-unity functions $g_{\text{nocol}}(\gamma)$ and $g_{\text{col}}(\gamma)$ are defined in Appendix B. They asymptote to $g_{\text{nocol}}(\gamma \rightarrow \infty) = g_{\text{col}}(\gamma \rightarrow \infty) = 10$.

4.2. Numerical solutions

Figure 2 shows a numerical integration of the equations of motion in the collisionless case ($s = \infty$), initialized with the collisionless self-similar solution (Equation B8) at scaled time $\tau = 1$. It is apparent from the figure that the evolution remains self-similar at all times, and agrees with the analytic expression (Equation (B8)). The mass distribution per logarithmic bin is indeed constant, in agreement with Equation (17).

Figure 3 shows an integration for the collisional case. It is initialized with Equation (B12) at $\tau = 1$, has $s = 0.1\alpha \times R_{\text{tran}}|_{\tau=1}$, and other parameters as before. The numerical integration agrees with the analytic expression, and shows that the mass distribution is top-heavy with $dN/dR \propto R^{-3}$ (Equation (17)).

In Figure 4, we experiment with a more commonly adopted initial spectrum—one that is more strongly peaked at a single size ($R = 1$). We perform two integrations, both of which have $\alpha = 10^{-4}$, $s = 1$ (i.e., s is the same as the location of the peak in the initial size distribution), and initially $N \propto R^{-7}$ at $R > 1$. The two integrations differ in the initial u : one has initial velocity equal to the escape speed of bodies with $R = 1$, and the other has u ten times lower. Over time, both converge to the collisional self-similar solution. The low u

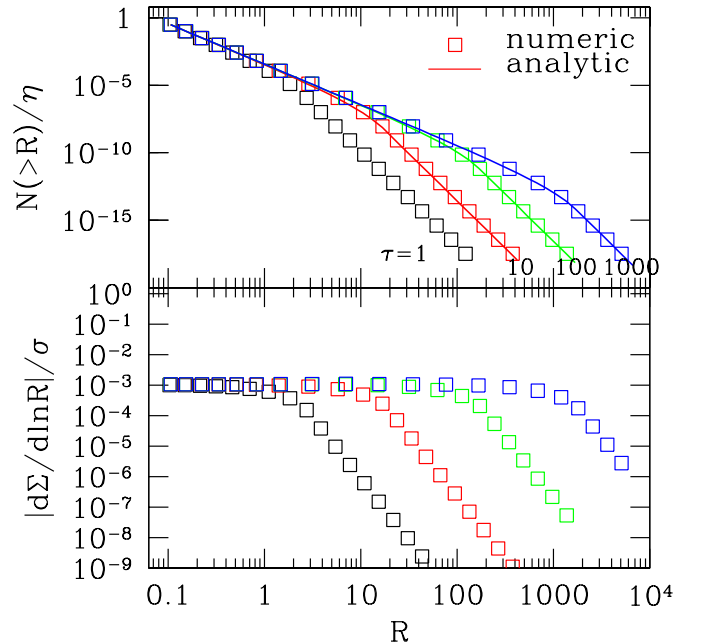


Figure 2. Collisionless evolution of Equations (4)–(7), initialized with the self-similar size distribution at scaled time $\tau \equiv \tau\Omega/(\rho\alpha) = 1$; R is measured in units of the initial value of R_{tran} . *Top panel:* The cumulative number distribution of big bodies (normalized by constant η) is plotted at three subsequent times. The numerical and analytic self-similar solutions agree. The initial parameters are $s = \infty$, $\alpha = 10^{-4}$, and $\gamma = 7$, i.e., $N \propto R^{-7}$ at large R . *Bottom panel:* The differential mass distribution, derived from the top panel via Equation (7). At each time, the radius of bodies that dominate stirring (R_{stir}) is near the break in N (or Σ) from one power-law slope to the other, and the small body speed is such that u is trans-hill relative to those stirring bodies (i.e., $R_{\text{tran}}/R_{\text{stir}} = \text{order-unity constant}$). Collisionless evolution leads to a size spectrum $dN/dR \propto R^{-4}$ at sizes below $\ln R_{\text{stir}}$, and the efficiency of forming large bodies is low, $d(\Sigma/\sigma)/d \ln R \sim 10\alpha$.

case undergoes a temporary phase of collisionless trans-hill growth, when the big bodies have yet to grow to $R \geq s/\alpha$. By contrast, the high u case takes longer to reach the trans-hill solution because its initial condition is more discrepant from trans-hill. In fact, this case completely skips the collisionless trans-hill regime. We have also experimented with different values for the initial power-law slope of N . The main resulting difference is the value of R at which the collisionless trans-hill solution commences. For example, when $N \propto R^{-5}$ at $R > 1$ (rather than R^{-7} as in Figure 4), then the high u solution follows the collisionless theory from $R = 10^{2.5}-10^4$.

In summary, as long as the evolution is collisionless, the efficiency of forming big bodies is small, with $\Sigma/\sigma \simeq 10\alpha$, independent of R . But once the evolution becomes collisional ($R_{\text{stir}} > s/\alpha$), the efficiency grows towards unity as R_{stir} increases.

5. AFTER TRANS-HILL GROWTH

5.1. Growth by accreting big bodies: Equal accretion

One of the ways trans-hill growth can end is when accretion of big bodies becomes important, violating assumption 3 in Section 2. To establish when that occurs, we calculate the accretion rate of big bodies, which requires knowing the big bodies' random speed v . Balancing dynamical friction damping due to small bodies with

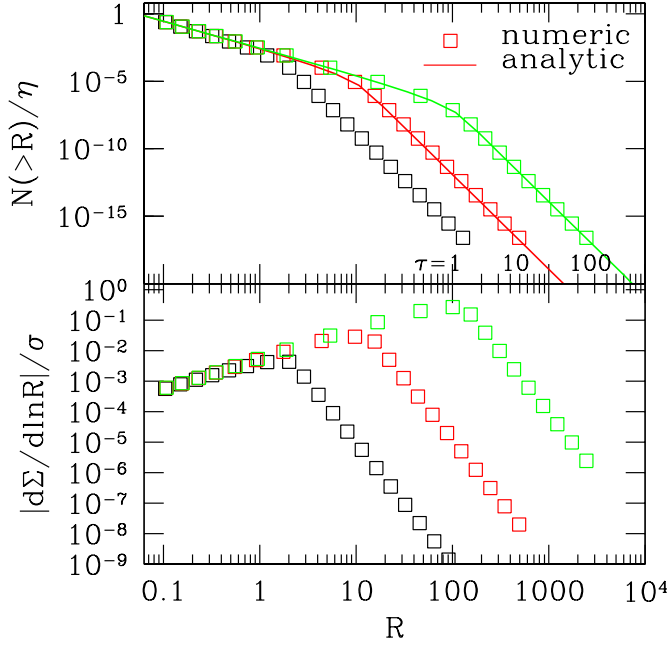


Figure 3. Collisional evolution: Similar to Figure 2, but showing the collisional case with parameters $s = 0.1\alpha$ (in units where the initial $R_{\text{tran}} = 1$) and, as before, $\alpha = 10^{-4}$ and $\gamma = 7$. The size spectrum is $dN/dR \propto R^{-3}$ at sizes below R_{stir} , and the efficiency of forming large bodies is much higher than the collisionless case.

viscous stirring due to other big bodies yields (GLS)

$$\frac{1}{v} \frac{dv}{dt} \sim \frac{\Omega}{\rho R} \alpha^{-2} \left(-\sigma + \Sigma \frac{v_H}{v} \right) \sim 0, \quad (20)$$

Therefore $v/v_H \sim \Sigma/\sigma \ll 1$. The growth rate by accreting big bodies with $v < v_H$ is (Rafikov 2003a, GLS)

$$\frac{1}{R} \frac{dR}{dt} \Big|_{\text{big}} \sim \frac{\Sigma \Omega}{\rho R} \alpha^{-3/2}, \quad (21)$$

which is larger than the usual (isotropic) sub-hill accretion formula (e.g., Equation (4)) because big bodies lie in a zero-inclination disk. Comparing growth by accreting big bodies with that by accreting small bodies,

$$\begin{aligned} \frac{d \ln R / dt \Big|_{\text{big}}}{d \ln R / dt \Big|_{\text{small}}} &\sim \frac{\Sigma}{\sigma} \alpha^{-1/2} \\ &\sim \begin{cases} \alpha^{1/2}, & \text{collisionless} \\ \alpha^{3/2} R_{\text{stir}} / s, & \text{collisional} \end{cases} \end{aligned} \quad (22)$$

using the trans-hill expressions. We conclude that in the collisionless regime it is always safe to ignore accretion by big bodies, in disagreement with Schlichting & Sari (2011) (see also Section 7). However, in the collisional regime, big body accretion becomes important once R_{stir} exceeds a critical value

$$\begin{aligned} R_{\text{stir}} &\gtrsim R_{\text{stir}}^{(\text{b.b. accrete})} = s \alpha^{-3/2} \\ &\approx 2800 \text{ km} \left(\frac{s}{1 \text{ km}} \right) \left(\frac{a}{1 \text{ AU}} \right)^{3/2} \end{aligned} \quad (24)$$

This occurs at time $t \sim \alpha^{-1/2} \rho s / (\sigma \Omega)$, and at that time the fraction of mass in big bodies (i.e., the efficiency) is $\Sigma/\sigma \sim \alpha^{1/2} \sim 7\% (a/1 \text{ AU})^{-1/2}$.

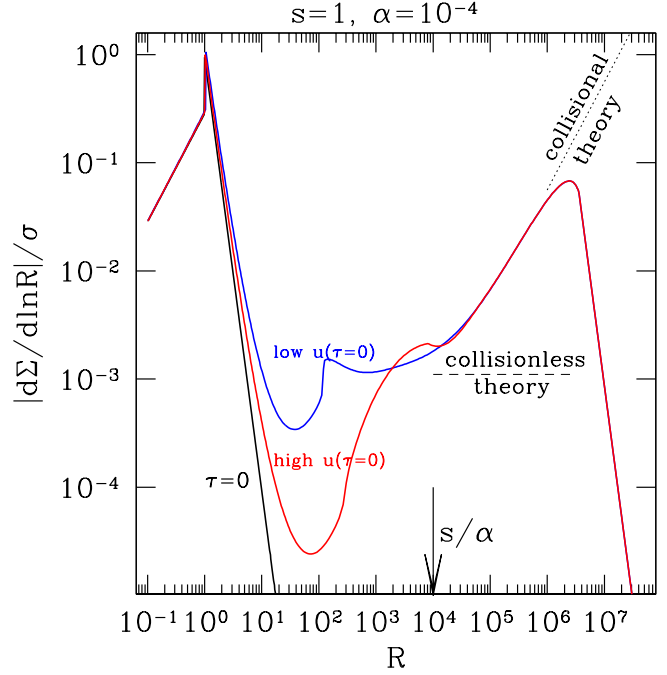


Figure 4. From runaway to trans-hill. Two integrations were initialized with nearly all bodies at the same size, $R = 1$ (the black profile marked $\tau = 0$). Numerical integrations of the equations of motion are plotted at scaled time $\tau = 2.5 \times 10^6$. For the red (high u) curve, the initial u is the surface escape speed from bodies with $R = 1$ (i.e., $R_{\text{tran}} = 1/\sqrt{\alpha} = 100$); for the blue curve, it is ten times smaller ($R_{\text{tran}} = 10$). Both integrations begin in the runaway stage, and converge onto the collisional self-similar solution (Equation (19), dotted line) when $R \gtrsim s/\alpha$ (Equation (14)). The low u case follows the collisionless solution (Equation (18), dashed line) for some time before collisional cooling becomes important. This explains the flat mass spectrum from $R = 10^2 - 10^4$. The high u case takes longer to reach the self-similar solution because its initial conditions differ more from the trans-hill state; in fact, it effectively skips the collisionless solution entirely.

As shown in Shannon et al. (2013b), after collisional trans-hill accretion ends, an epoch of “equal accretion” begins, during which big bodies grow by accreting comparable mass in big and in small bodies. Equal accretion terminates when half of the mass has been converted into big bodies, $\Sigma \sim \sigma$.

The scenario outlined above is applicable as long as oligarchy has not yet begun. We discuss oligarchy next.

5.2. Oligarchic Growth

As accretion proceeds, the number of stirring bodies decreases, and hence neighboring stirrers become increasingly separated. Eventually, they become so separated that each small body is predominantly stirred by, and accreted onto, a single big body. When that happens, assumption 5 is violated (Section 2) and oligarchy commences (Kokubo & Ida 1998, GLS). In oligarchy, the nature of growth is modified. Instead of a continuous size spectrum, the largest body in each radial annulus separates from the size spectrum of smaller bodies. The velocity dispersion u is no longer trans-hill.

The value of R_{stir} at which oligarchy starts depends on the size spectrum, for which we now have a simple model. For trans-hill velocity dispersion, oligarchy begins when the separation between adjacent big bodies ($\Delta a \sim \rho R^3 / (a \Sigma)$) exceeds their Hill radius ($R_H \sim R/\alpha$).

If we define the oligarchy parameter

$$\begin{aligned} \text{OP} &\equiv \frac{\Delta a}{R_H} \\ &= \frac{\rho \alpha R^2}{\Sigma a}, \end{aligned} \quad (25)$$

then oligarchy begins when $\text{OP} \sim 1$. Inserting the efficiency of big body formation (Equation (14)) into the above, we find that trans-hill growth transitions to oligarchy once R_{stir} exceeds

$$R_{\text{stir}}^{(\text{oligarchy})} \approx \begin{cases} \sqrt{\frac{\sigma a}{\rho}} \approx 150 \text{ km} \cdot \sigma_{16}^{1/2} \left(\frac{a}{1 \text{ AU}}\right)^{1/2}, & \text{collisionless} \\ \left(\frac{\alpha}{s}\right) \frac{\sigma a}{\rho} \approx 120 \text{ km} \cdot \sigma_{16} \left(\frac{s}{1 \text{ km}}\right)^{-1}, & \text{collisional} \end{cases} \quad (26)$$

where $\sigma_{16} \equiv \sigma / (16 \text{ g/cm}^2)$. For the MMSN density profile, $\sigma_{16} \approx (a/1 \text{ AU})^{-3/2}$ with an enhancement beyond the snow line by a factor of ~ 5 . The collisionless expression above applies as long $R_{\text{stir}}^{(\text{oligarchy})} < R_{\text{stir}}^{(\text{col})} \approx s/\alpha$; otherwise the collisional one applies. However, we caution that depending on parameter values the equal accretion stage discussed in Section 5.1 may begin earlier than oligarchy, which would lead to a different transition criterion.

Once oligarchy takes hold, neighboring regions evolve independently under the stirring of their respective oligarchs, as discussed in Sections 9-10 of GLS. Neighboring oligarchs likely converge in size, their battling leading to scattering or merging. The evolution depends to a large degree on the fate of the small bodies. At late times, small bodies collide at such high speeds that they almost certainly fragment. As the small bodies grind down each other, the evolution can become increasingly collisional. The small bodies may cool and the oligarchs may carve gaps around themselves, effectively sabotaging their accretion (Rafikov 2003b; Levison et al. 2010). We defer considerations of these dynamics to future work.

If the oligarchs eventually reach the isolation mass, they may undergo orbital instability and experience giant impacts. The timescale to form planets of size R is

$$t_{\text{impact}} \approx \frac{\rho R}{\Sigma \Omega} \sim 10^8 \left(\frac{R}{R_{\oplus}}\right) \sigma_{16}^{-1} \left(\frac{a}{1 \text{ AU}}\right)^{3/2} \text{ yrs}, \quad (27)$$

which is very long in the outer solar system.

Our criterion for oligarchy ($\text{OP} \sim 1$) differs from that of Ormel et al. (2010a). They stipulate, based on empirical evidence from Monte Carlo simulations, that oligarchy begins when the stirring rate by one single large body equals its growth rate, and that, in turn equals the small body collision rate. Their definition of oligarchy differs from ours: their oligarchy begins when the ratio of small body random velocity to Hill velocity of the biggest body reaches a minimum. In fact, their oligarchy is similar to (but still somewhat different from) the trans-hill phase. To some extent, this is a matter of how one defines oligarchy. But irrespective of definitions, there should be a transition from trans-hill to oligarchic behavior when $\Delta a \sim R_H$.

6. EXAMINING ASSUMPTIONS

We examine the assumptions made in deriving the properties of trans-hill growth (Section 2):

1. The requirement that u satisfies Equation (1) is equivalent to insisting that we only consider big bodies with $\alpha^{1/2} < R/R_{\text{tran}} < \alpha^{-1/2}$. Bodies that violate these restrictions grow more slowly than Equation (4) predicts (Goldreich et al. 2004b), but this has little effect on trans-hill growth.
2. The assumption that $v/v_H < 1$ is confirmed by Equation (20).
3. We ignored growth by accretion of big bodies. When that assumption is violated, equal accretion begins (Section 5.1).
4. We assumed that s is constant. In truth, at late times u can become sufficiently large that collisions between small bodies fragment them. We do not treat this in detail because the physics of fragmentation is complex. We note, however, that since bodies of smaller sizes are typically more resistant to fragmentation (for $s \ll 1 \text{ km}$), the result of fragmentation is likely that s is a decreasing function of the stirring bodies' sizes. This will alter the spectrum of trans-hill accretion (Equation (14)) in that one should replace the s in that equation with the function $s(R_{\text{stir}})$. A similar remark applies to other mechanisms for damping u , such as gas drag. Since s only appears in the equations of motion through its damping effect on u , gas drag may also be modelled by adopting a much smaller effective s .
5. We ignored oligarchy. The transition to oligarchic stage is described in Section 5.2.

7. APPLICATIONS AND COMPARISONS

7.1. The Asteroid Belt

Here we compare our results with published coagulation simulations for the asteroid belt. At a distance of 2 AU, $\alpha \approx 2.5 \times 10^{-3}$, so the transition from collisionless to collisional evolution occurs when large bodies grow beyond $s/\alpha \sim 400 \text{ km}(s/1 \text{ km})$.

The uppermost end of the asteroid mass distribution is roughly flat, i.e. $d\Sigma/d \ln R \sim \text{const}$ for $100 \text{ km} \lesssim R \lesssim 300 \text{ km}$. But for $R \lesssim 100 \text{ km}$, Σ falls off with decreasing R (Jedicke et al. 2002; Bottke et al. 2005, taking a constant albedo of 0.04). Both Morbidelli et al. (2009) and Weidenschilling (2011) attempt to reproduce the observed distribution, including the 100km ‘‘bump,’’ by running particle-in-a-box coagulation simulations that are initialized with single-sized small planetesimals. But the two reach opposite conclusions. Morbidelli et al. (2009), with small planetesimal sizes ranging from $s = 0.6$ to 6 km, fail to produce the 100km bump: the final distributions they find are roughly flat ($q \sim 4$) for a range in R that extends an order of magnitude below 100km. But Weidenschilling succeeds when using $s \approx 0.1 \text{ km}$. He attributes the difference to the erroneous neglect of sub-hill accretion by Morbidelli et al. In the following, we focus on explaining Weidenschilling’s results.⁵

⁵ An additional difference between the simulations of Morbidelli et al. (2009) and Weidenschilling (2011) is that the former initialize velocities to be the Hill velocity of the initial bodies, whereas the latter initialize them to be the escape speed. This might tend to flatten out the post-runaway bump in the simula-

Weidenschilling’s bump at 100km appears to be due to the transition from runaway to collisional trans-hill growth. These simulations resemble the red curve in Fig. 4—with a transition directly from runaway to collisional trans-hill—because the initial velocity is the escape speed from seeds. And like the red curve that shows a transition around $R \sim s/\alpha$, the final size distribution in Weidenschilling (2011) also shows a bump around 50km (his Fig. 8), produced when the small body dispersion goes from super-hill (runaway) to trans-hill. The value of Σ/σ at the location of his bump, and the slope to the right of the bump, are all roughly consistent with what we derive in this paper.

If the observed 100km bump in the asteroid belt is indeed produced by the transition from runaway to trans-hill growth, that would imply that the initial mass of small planetesimals, relative to that in current big bodies, was at least $\sigma/\Sigma \sim 1/(10\alpha) \sim 50$ times greater (Equation (18))—or even greater if some asteroids were dynamically ejected (Morbidelli et al. 2009). It would also imply that the initial small bodies had radii $\sim \alpha \times 100\text{km} \sim 0.2\text{km}^6$. One interesting implication of such a scenario is that the vast majority of these small bodies could not be dynamically ejected, because if they were that would correspondingly reduce the number of big bodies too. Instead, they had to be ground down to dust which was then eliminated by radiation forces. Whether this can occur has yet to be examined carefully. But we note that by the time the asteroids grew to $\sim 100\text{km}$, the small bodies would have begun to collide with one another with collision speeds $v_H|_{R=100\text{km}} \sim 5\text{m/sec}$. Such speeds might have been sufficient to grind all the planetesimals and eliminate them, preventing further growth of asteroids.

7.2. The Kuiper Belt

With a value of $\alpha \approx 10^{-4}$ for the Kuiper belt, the transition to trans-hill collisional growth occurs at $10^4\text{km}(s/1\text{km})$. So with the typical choice $s = 1\text{km}$ and the largest bodies observed at 1000 km, there is little wonder that simulations to date have not probed the collisional regime (but see Shannon et al. 2013b).

Kenyon & Luu (1999) perform particle-in-box simulations for the formation of Kuiper belt objects. Starting from bodies of size $s = 80\text{m}$, their simulations produce big bodies with a flat mass distribution ($q = 4$) for $3\text{km} \lesssim R \lesssim 1000\text{km}$ (see, e.g. their Fig. 8). This is roughly consistent with the observed mass distribution in the Kuiper belt at large sizes (e.g., Fraser et al. 2010), and hence may be taken as evidence that the formation of Kuiper belt objects has been solved. However, recent data have cast doubt on such a simple picture (Shankman et al. 2012).

Our theory explains some aspects of Kenyon & Luu’s simulations. The growth they witness should entirely be in the collisionless regime, and the mass spectrum should be flat, as indeed they observe. However, the efficiency that they find is $\sim 1\%$, whereas we predict $\sim 10\alpha \sim 0.1\%$. We have been unable to resolve this

tions of Morbidelli et al., similar to how, in Figure 4, the blue curve is flatter than the red.

⁶ The initial small body radii would be less than 0.2 km by a factor of ~ 5 if the MMSN budget of gas was still present when the bump was formed (e.g., GLS).

discrepancy. In Shannon et al. (2013a), we repeat their simulations and find an efficiency of $\sim 0.1\%$.

Schlichting & Sari (2011) consider collisionless coagulation both analytically and with numerical simulations. They conclude that the flat mass spectrum obtained in collisionless simulations arises because big bodies grow equally by accreting big and small bodies (“equal accretion”). By contrast, we have shown that it is due to trans-hill growth. In fact, Equation (23) shows that trans-hill growth in the collisionless regime prevents equal accretion from occurring. Nonetheless, the efficiency they derive ($\alpha^{3/4}$), happens to be close in numerical value to our efficiency of 10α for Kuiper belt parameters. In Shannon et al. (2013a), we confirm with numerical simulations that account for order-unity coefficients that it is trans-hill growth rather than equal accretion that sets the size spectrum in the collisionless regime.

A troubling concern with low-efficiency collisionless growth of KBOs is that one needs to grind down 99.9% of the small bodies to dust and blow it out with radiation pressure. As we show in an upcoming paper, this is almost impossible to do. This concern is alleviated if the initial planetesimal size is significantly smaller than 1 km. The formation efficiency can then be significantly boosted by collisional growth (Shannon et al. 2013b).

7.3. Ormel et al. (2010b)

Ormel et al. (2010b) perform a comprehensive study of conglomeration, at semimajor axes ranging from 1 AU to 35AU. Their numerical algorithm allows them to follow the evolution from runaway through oligarchy. We observe that there is a distinct trans-hill phase in their simulations (e.g., Figs. 8 & 11 of that paper). With their parameters of $s = 7.5\text{km}$, $\sigma = 16\text{g/cm}^2$, one expects the transhill evolution (collisionless below $R_{\text{stir}} = 1500(a/1\text{AU})\text{km}$) to lead to a characteristic size spectrum of $q = 4$ and a formation efficiency of $\Sigma/\sigma \sim 0.05(a/1\text{AU})$. These are indeed observed in their results.⁷ Above $R = 1500\text{km}(a/1\text{AU})$, the evolution is collisional. For some of their simulations (the ones at small a), oligarchy enters at around the same point. So instead of observing a continuous mass spectrum of $q = 3$ (Equation (17)), they find that a single body that grows to large sizes.

8. SUMMARY

Runaway growth ends once the stirring bodies become trans-hill ($v_H|_{\text{stir}} \sim u$, or equivalently $R_{\text{stir}} \sim u/\sqrt{G\rho\alpha}$). Afterwards, R_{stir} and u grow in unison, and the stirring bodies remain trans-hill. For $R_{\text{stir}} < s/\alpha$, trans-hill growth is collisionless. The mass spectrum is flat ($q = 4$), and the efficiency low, $\sim 10\alpha$. But for $R_{\text{stir}} > s/\alpha$, the evolution is collisional and the efficiency grows in proportion to R_{stir} , with a size spectrum that has $q = 3$. The time to reach the collisional transition is comparable to the small bodies’ collision time ($\rho s/\sigma\Omega$). Our numerical simulations and self-similar calculations confirm these results, subject to the assumptions made in Section 2.

⁷ Although Ormel et al. (2010b) fit their result with a power-law slope of $q = 5.5$ ($p = -2.5$ in their notation), it appears that the big bodies are better characterized by a flat mass distribution of $q = 4$ (see, e.g., their Fig. 13).

The simulations also show that where the collisionless trans-hill spectrum begins depends on the unknown initial conditions—especially the initial size spectrum and u . But the collisional trans-hill spectrum invariably begins once $R_{\text{stir}} > s/\alpha$.

Having described trans-hill growth, we briefly discussed what comes next, when one or more of the assumptions in Section 2 breaks. Collisional trans-hill growth ends once $R_{\text{stir}} \gtrsim s\alpha^{-3/2}$ (efficiency $\Sigma/\sigma \gtrsim \sqrt{\alpha}$), because once that happens mutual accretion of big bodies becomes important (Section 5). As we show in a forthcoming paper (Shannon et al. 2013b), this regime is characterized by equal accretion of big and small bodies, and can lead to order-unity efficiency. However, the mass spectrum below R_{stir} is no longer frozen, and hence if this regime is reached it can wipe out the mass spectrum laid down during trans-hill growth.

Trans-hill growth can also be terminated when big bodies become separated by a Hill radius, in which case oligarchy sets in. Another complication is collisional fragmentation. We leave more detailed consideration of these two effects to future work. On the other hand, the complication of gas damping is easily incorporated by using an effective s .

Our theory explains results from previous studies of the asteroid and Kuiper belt. Most simulations to date adopt parameters relevant for collisionless growth, typically with initial seeds $s \sim 1$ km. For the Kuiper belt, this means the growth is collisionless at all times and the efficiency is limited to $10\alpha \sim 0.1\%$. So if the Kuiper belt has been severely dynamically depleted, it would initially have had to contain multiple times the MMSN mass. Alternatively, the efficiency of formation can approach unity if the initial seed size is small. We explore how this may explain the formation of Kuiper belt in an upcoming publication.

We thank Yanqin Wu for useful discussions. We ac-

knowledge NSF grant AST-1109776.

REFERENCES

- Bottke, W. F., Durda, D. D., Nesvorný, D., et al. 2005, *Icarus*, 175, 111
- Chambers, J. E., & Wetherill, G. W. 1998, *Icarus*, 136, 304
- Chiang, E., & Youdin, A. N. 2010, *Annual Review of Earth and Planetary Sciences*, 38, 493
- Fraser, W. C., Brown, M. E., & Schwamb, M. E. 2010, *Icarus*, 210, 944
- Goldreich, P., Lithwick, Y., & Sari, R. 2004a, *ApJ*, 614, 497
- . 2004b, *ARA&A*, 42, 549, (GLS in text)
- Greenberg, R., Hartmann, W. K., Chapman, C. R., & Wacker, J. F. 1978, *Icarus*, 35, 1
- Ida, S., & Makino, J. 1993, *Icarus*, 106, 210
- Inaba, S., Tanaka, H., Nakazawa, K., Wetherill, G. W., & Kokubo, E. 2001, *Icarus*, 149, 235
- Jedicke, R., Larsen, J., & Spahr, T. 2002, *Asteroids III*, 71
- Johansen, A., Oishi, J. S., Low, M.-M. M., et al. 2007, *Nature*, 448, 1022
- Kenyon, S. J., & Luu, J. X. 1999, *AJ*, 118, 1101
- Kokubo, E., & Ida, S. 1998, *Icarus*, 131, 171
- Lee, M. H. 2000, *Icarus*, 143, 74
- Levison, H. F., Thommes, E., & Duncan, M. J. 2010, *AJ*, 139, 1297
- Malyskin, L., & Goodman, J. 2001, *Icarus*, 150, 314
- Morbidelli, A., Bottke, W. F., Nesvorný, D., & Levison, H. F. 2009, *Icarus*, 204, 558
- Ormel, C. W., Dullemond, C. P., & Spaans, M. 2010a, *ApJ*, 714, L103
- . 2010b, *Icarus*, 210, 507
- Pollack, J. B., Hubickyj, O., Bodenheimer, P., et al. 1996, *Icarus*, 124, 62
- Rafikov, R. R. 2003a, *AJ*, 126, 2529
- . 2003b, *AJ*, 125, 942
- Safronov, V. S. 1972, *Evolution of the protoplanetary cloud and formation of the earth and planets*. (NASA-TTF-677)
- Schlichting, H. E., & Sari, R. 2011, *ApJ*, 728, 68
- Shankman, C., Gladman, B., Kaib, N., Kavelaars, J. J., & Petit, J.-M. 2012, *ArXiv e-prints*
- Shannon, A., Wu, Y., & Lithwick, Y. 2013a
- Shannon, A., Lithwick, Y., & Wu, Y. 2013b
- Weidenschilling, S. J. 2011, *Icarus*, 214, 671
- Weidenschilling, S. J., Spaute, D., Davis, D. R., Marzari, F., & Ohtsuki, K. 1997, *Icarus*, 128, 429
- Wetherill, G. W., & Stewart, G. R. 1989, *Icarus*, 77, 330

APPENDIX

A. NUMERICAL SOLUTION OF THE EQUATIONS OF MOTION

In order to numerically integrate the equations of motion (Equations (4)–(7)), we first re-write the equations in terms of the trans-hill radius $R_{\text{tran}} \equiv u/\sqrt{G\rho\alpha}$ (Equation (10)) and the rescaled time,

$$\tau = \frac{\sigma\Omega}{\rho\alpha} t. \quad (\text{A1})$$

which has units of length. Equation (4) becomes

$$\frac{dR}{d\tau} = \begin{cases} (R/R_{\text{tran}})^2, & \text{if } R < R_{\text{tran}} \\ R/R_{\text{tran}}, & \text{if } R > R_{\text{tran}} \end{cases}, \quad (\text{A2})$$

and Equation (5), with the replacement of Equation (7), becomes

$$\frac{1}{R_{\text{tran}}} \frac{dR_{\text{tran}}}{d\tau} = -\frac{\alpha}{s} - \frac{1}{\alpha} \left(\int_{R < R_{\text{tran}}} \frac{R^6}{R_{\text{tran}}^4} \frac{dN}{\eta} + \int_{R > R_{\text{tran}}} \frac{R^3}{R_{\text{tran}}} \frac{dN}{\eta} \right) \quad (\text{A3})$$

The continuity equation (Equation (6)) becomes

$$\partial_\tau N + V \partial_R N = 0, \quad (\text{A4})$$

where $V \equiv dR/d\tau$ is given by equation (A2).

Our numerical method is as follows. We choose an initial value for R_{tran} and an initial form for the function $N(> R)$ on a logarithmic grid in R , where the grid typically has 400 gridpoints per decade of R . According to Equation (A4), the value of N remains constant at any R that satisfies Equation (A2). Therefore, for each initial N on the grid, we integrate its corresponding R according to Equation (A2). We simultaneously evolve R_{tran} according to Equation (A3).

B. SELF-SIMILAR SOLUTIONS

If one considers either the collisionless or the collisional case, then there is only a single characteristic radius, R_{tran} . Therefore, Equation (A4) may be written in self-similar form when appropriately scaled. We define the scaled independent variable to be the ratio of R to its characteristic value,

$$x \equiv R/R_{\text{tran}}(\tau), \quad (\text{B1})$$

and the scaled dependent variable to be

$$y(x) \equiv R_{\text{tran}}^p N(R, \tau)/\eta, \quad (\text{B2})$$

with p to be determined below. In scaled variables, Equation (A4) becomes

$$\frac{dR_{\text{tran}}}{d\tau} \left(x \frac{dy}{dx} + py \right) = V(x) \frac{dy}{dx}, \quad (\text{B3})$$

where

$$V(x) = \begin{cases} x^2, & \text{if } x < 1 \\ x, & \text{if } x > 1 \end{cases}. \quad (\text{B4})$$

Self-similarity demands

$$\frac{dR_{\text{tran}}}{d\tau} = A \Rightarrow R_{\text{tran}} = A\tau \quad (\text{B5})$$

where A is a constant to be determined. Substituting into Equation (B3), we may solve for y to obtain

$$y(x) = y(1) \begin{cases} x^{-p}(A-x)^p/(A-1)^p, & x < 1 \\ x^{-pA/(A-1)}, & x > 1 \end{cases}, \quad (\text{B6})$$

where we must have $A > 1$. Equation (A3) becomes

$$\frac{A}{R_{\text{tran}}} = -\frac{\alpha}{s} - \frac{1}{\alpha} R_{\text{tran}}^{2-p} \left(\int_{x<1} x^6 dy + \int_{x>1} x^3 dy \right). \quad (\text{B7})$$

It remains to determine the three constants $p, A, y(1)$. To do so, we consider the collisionless and collisional cases separately.

In the collisionless case, $\alpha/s \ll A/R_{\text{tran}}$. This is equivalent to the condition $t \ll \rho s/(\sigma\Omega)$, i.e., that the time elapsed is less than the collision time between small bodies. Equation (B7) demands that $p = 3$ since A is a constant in time, i.e., $N/\eta = y(x)/R_{\text{tran}}^3$. Note that since N is frozen (independent of time) at small x (i.e. for $R \ll R_{\text{tran}}$), this immediately implies that $N \propto R^{-3}$ for $R \ll R_{\text{tran}}$. Integrating Equation (B7) yields a relation between the remaining two constants, $y(1)$ and A . We write the resulting self-similar solution as follows:

$$\frac{N(> R, t)}{\eta} = \frac{\alpha}{R_{\text{tran}}^3} g_{\text{nocol}}(\gamma) f_3 \left(\frac{R}{R_{\text{tran}}}, \gamma \right), \text{ collisionless}, \quad (\text{B8})$$

where

$$R_{\text{tran}}(t) = \frac{\sigma\Omega}{\rho\alpha} \frac{t}{1 - 3/\gamma} \quad (\text{B9})$$

$$g_{\text{nocol}}(\gamma) \equiv \frac{10\gamma^3}{\gamma^3 + 6\gamma^2 + 27\gamma + 108} \quad (\text{B10})$$

$$f_p(x, \gamma) \equiv \begin{cases} x^{-p} \left(1 - x(1 - \frac{p}{\gamma}) \right)^p, & x < 1 \\ x^{-\gamma} \left(\frac{p}{\gamma} \right)^p, & x > 1 \end{cases}. \quad (\text{B11})$$

In the collisional case ($\alpha/s \gg A/R_{\text{tran}}$), Equation (B7) implies that $p = 2$, which yields $N \propto R^{-2}$ for $R \ll R_{\text{tran}}$. Integrating Equation (B7) yields the self-similar solution

$$\frac{N(> R, t)}{\eta} = \frac{1}{R_{\text{tran}}^2} \frac{\alpha^2}{s} g_{\text{col}}(\gamma) f_2 \left(\frac{R}{R_{\text{tran}}}, \gamma \right), \text{ collisional} \quad (\text{B12})$$

where

$$R_{\text{tran}} = \frac{\sigma\Omega}{\rho\alpha} \frac{t}{1 - 2/\gamma} , \quad (\text{B13})$$

$$g_{\text{col}}(\gamma) \equiv \frac{10\gamma(\gamma - 3)}{\gamma^2 + 5\gamma + 16} \quad (\text{B14})$$

and $f_p(x, \gamma)$ is by Equation (B11).